Time Domain Flutter and Buffeting Response Analysis of Bridges

By Xinzhong Chen,[1] Masaru Matsumoto,[2] and Ahsan Kareem[3]

ABSTRACT: A time domain approach for predicting the coupled flutter and buffeting response of long span bridges is presented. The frequency dependent unsteady aerodynamic forces are represented by the convolution integrals involving the aerodynamic impulse function and structural motions or wind fluctuations. The aerodynamic impulse functions are derived from experimentally measured flutter derivatives, aerodynamic admittance functions, and spanwise coherence of aerodynamic forces using rational function approximations. A significant feature of the approach presented here is that the frequency dependent characteristics of unsteady aerodynamic forces and the nonlinearities of both aerodynamic and structural origins can be modeled in the response analysis. The flutter and buffeting response of a long span suspension bridge is analyzed using the proposed time domain approach. The results show good agreement with those from the frequency domain analysis. The example used to demonstrate the proposed scheme focuses on the treatment of frequency dependent self-excited and buffeting force effects. Application to nonlinear effects will be addressed in a future publication.

INTRODUCTION

The prediction of wind induced buffeting response and flutter instability is of major concern in the design of long span bridges. The analytical approach has predominantly been conducted in the frequency domain (Davenport 1962; Scanlan 1978). This is primarily due to the computational efficiency offered by the frequency domain, particularly when handling the unsteady aerodynamic forces that are functions of frequency. The flutter analysis is generally conducted by complex eigenvalue analysis, whereas the buffeting response is typically estimated using a mode-by-mode approach that ignores the aerodynamic coupling among modes. More recently, an efficient scheme for coupled multimode flutter analysis has been proposed by introducing the unsteady self-excited aerodynamic forces in terms of rational function approximations (Matsumoto et al. 1994; Chen et al. 2000). This has led to a convenient transformation of the equations into a frequency independent state-space format. A significant feature of this approach is that an iterative solution for determining flutter conditions is unnecessary because the equations of motion are independent of frequency. The effects of aerodynamic coupling on the buffeting response have been addressed by the studies (Matsumoto et al. 1994; Jain et al. 1996; Katsuchi et al. 1999; Chen et al. 2000). In general, the frequency domain approach is restricted to linear structures excited by the stationary wind loads without aerodynamic nonlinearities.

To include nonlinearities of structural and aerodynamic origins, the time domain approach is more appropriate. In the following studies, among others, the time domain approach has been utilized for the analysis of flutter and buffeting response [e.g., Agar (1988), Kovacs et al. (1992), Santos et al. (1993), Matsumoto et al. (1994), Xiang et al. (1995), and Diana et al. (1998)]. Most of the previous studies concerning the buffeting response have used the quasi-steady theory for modeling the aerodynamic forces, thus ignoring the frequency dependent characteristics of unsteady aerodynamic forces in the

[1]Postdoctoral Res. Assoc., NatHaz Modeling Lab., Dept. of Civ. Engrg. and Geological Sci., Univ. of Notre Dame, Notre Dame, IN 46556.

[2]Prof., Dept. of Global Environment Engrg., Kyoto Univ., Kyoto 606-8501, Japan.

[3]Prof. and Chair, Dept. of Civ. Engrg. and Geological Sci., Univ. of Notre Dame, Notre Dame, IN.

numerical scheme. Time domain approaches also require input time histories of multidimensional multivariant wind fields. They can be simulated using a spectral or time series approach [e.g., Sinozuka and Jan (1972) and Li and Kareem (1993)].

In this paper, a time domain approach for predicting the flutter and buffeting response utilizing frequency dependent unsteady aerodynamic forces is presented. A significant feature of this approach is that the frequency dependent characteristics of unsteady aerodynamic forces and nonlinearities of both aerodynamic and structural origins can be taken into account when estimating the response. The flutter and buffeting response of a suspension bridge with a main span of approximately 2,000 m is used to demonstrate the effectiveness of the proposed scheme. The results are compared with the frequency domain approach. The effects of aerodynamic coupling induced by the coupled self-excited forces and unsteady characteristics of buffeting forces are also investigated.

THEORETICAL BACKGROUND

Analysis of Full-Order System

The governing equations of motion with respect to the static equilibrium position of a bridge excited by aerodynamic forces are given in a matrix form by

$$\mathbf{M\ddot{Z}} + \mathbf{C\dot{Z}} + \mathbf{KZ} = \mathbf{F}_{se} + \mathbf{F}_{b} \qquad (1)$$

where $\mathbf{M}$, $\mathbf{C}$, and $\mathbf{K}$ = mass, damping, and stiffness matrices, respectively; $\mathbf{Z}$ = nodal displacement vector; $\mathbf{F}$ indicates the nodal force vector; each dot denotes the partial differentiation with respect to time t; and the subscripts se and b represent the self-excited and turbulence-induced buffeting force components, respectively.

For the harmonic motion, the self-excited forces per unit span (Fig. 1) [i.e., lift $L_{se}(t)$, drag $D_{se}(t)$, and pitching moment $M_{se}(t)$] are commonly described utilizing flutter derivatives as follows (Scanlan 1978):
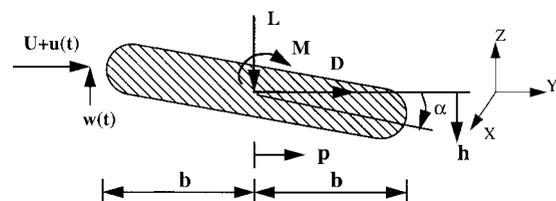

FIG. 1. Aerodynamic Forces on Bridge Section

$$L_{se}(t) = \frac{1}{2} \rho U^2 (2b) \left(k H_1^* \frac{\dot{h}}{U} + k H_2^* \frac{b\dot{\alpha}}{U} + k^2 H_3^* \alpha + k^2 H_4^* \frac{h}{b} \right.$$

$$\left. + k H_5^* \frac{\dot{p}}{U} + k^2 H_6^* \frac{p}{b} \right) \tag{2a}$$

$$D_{se}(t) = \frac{1}{2} \rho U^2 (2b) \left(k P_1^* \frac{\dot{p}}{U} + k P_2^* \frac{b\dot{\alpha}}{U} + k^2 P_3^* \alpha + k^2 P_4^* \frac{p}{b} \right.$$

$$\left. + k P_5^* \frac{\dot{h}}{U} + k^2 P_6^* \frac{h}{b} \right) \tag{2b}$$

$$M_{se}(t) = \frac{1}{2} \rho U^2 (2b^2) \left(k A_1^* \frac{\dot{h}}{U} + k A_2^* \frac{b\dot{\alpha}}{U} + k^2 A_3^* \alpha + k^2 A_4^* \frac{h}{b} \right.$$

$$\left. + k A_5^* \frac{\dot{p}}{U} + k^2 A_6^* \frac{p}{b} \right) \tag{2c}$$

where ρ = air density; U = mean wind velocity; $k = \omega b/U$ = reduced frequency; $B = 2b$ = bridge deck width; ω = circular frequency of vibration; H_i^*, P_i^*, and A_i^* ($i = 1-6$) = frequency dependent flutter derivatives; h, p, and α = vertical, lateral, and torsional displacement, respectively.

The self-excited forces per unit span induced by arbitrary structural motion can be expressed in terms of convolution integrals as follows (Lin and Yang 1983):

$$L_{se}(t) = \frac{1}{2} \rho U^2 \int_{-\infty}^{t} (I_{L_{seh}}(t - \tau) h(\tau) + I_{L_{sep}}(t - \tau) p(\tau)$$

$$+ I_{L_{se\alpha}}(t - \tau) \alpha(\tau)) \, d\tau \tag{3a}$$

$$D_{se}(t) = \frac{1}{2} \rho U^2 \int_{-\infty}^{t} (I_{D_{seh}}(t - \tau) h(\tau) + I_{D_{sep}}(t - \tau) p(\tau)$$

$$+ I_{D_{se\alpha}}(t - \tau) \alpha(\tau)) \, d\tau \tag{3b}$$

$$M_{se}(t) = \frac{1}{2} \rho U^2 \int_{-\infty}^{t} (I_{M_{seh}}(t - \tau) h(\tau) + I_{M_{sep}}(t - \tau) p(\tau)$$

$$+ I_{M_{se\alpha}}(t - \tau) \alpha(\tau)) \, d\tau \tag{3c}$$

where I indicates the impulse function of the self-excited forces, which are associated with indicial aerodynamic functions (Scanlan et al. 1974; Scanlan 1984), and the subscripts represent the corresponding force components.

The relationship between the aerodynamic impulse functions and flutter derivatives can be obtained by taking the Fourier transform of (3) and comparing to the corresponding terms in (2)

$$\bar{I}_{L_{seh}} = 2k^2 (H_4^* + iH_1^*); \quad \bar{I}_{L_{sep}} = 2k^2 (H_6^* + iH_5^*);$$

$$\bar{I}_{L_{se\alpha}} = 2k^2 b (H_3^* + iH_2^*) \tag{4a}$$

$$\bar{I}_{D_{seh}} = 2k^2 (P_6^* + iP_5^*); \quad \bar{I}_{D_{sep}} = 2k^2 (P_4^* + iP_1^*);$$

$$\bar{I}_{D_{se\alpha}} = 2k^2 b (P_3^* + iP_2^*) \tag{4b}$$

$$\bar{I}_{M_{seh}} = 2k^2 b (A_4^* + iA_1^*); \quad \bar{I}_{M_{sep}} = 2k^2 b (A_6^* + iA_5^*);$$

$$\bar{I}_{M_{se\alpha}} = 2k^2 b^2 (A_3^* + iA_2^*) \tag{4c}$$

where the overbar denotes the Fourier transform operator; and terms containing i represent imaginary parts.

In light of (3), the self-excited forces can be described in the frequency domain as a product of the bridge displacement and the corresponding transfer function, which has been expressed in terms of flutter derivatives [(4)]. Because the flutter derivatives are normally known only at discrete values of the reduced frequency k, approximate expressions are used to develop these as continuous functions of the reduced frequency

for future analysis. The rational function approximation approach known as Roger's approximation can be utilized for this purpose (Roger 1977). With regard to the term corresponding to the lift induced by the vertical motion $L_{seh}(t)$, the aerodynamic transfer function can be expressed as

$$\bar{I}_{L_{seh}}(i\omega) = 2k^2 (H_4^* + iH_1^*) = A_1 + A_2 \left(\frac{i\omega b}{U} \right) + A_3 \left(\frac{i\omega b}{U} \right)^2$$

$$+ \sum_{l=1}^{m} \frac{A_{l+3} i\omega}{i\omega + \frac{d_l U}{b}} \tag{5}$$

where A_1, A_2, A_3, A_{l+3}, and d_l ($d_l \geq 0$; $l = 1$ to m) are frequency independent coefficients; the first and second terms represent noncirculatory static-aerodynamics and the aerodynamic damping, respectively; the third term denotes the additional aerodynamic mass that is normally negligible; and the rational terms represent the unsteady components that lag the velocity term and permit an approximation of the time delays through positive values of the parameter d_l. The value of m determines the level of accuracy of this approximation and the size of additional equations [given in (8)]. All of the coefficients in (5) can be determined by the linear and nonlinear least-squares methods using the experimentally obtained flutter derivatives at different reduced frequencies.

The preceding rational function representation of the aerodynamic transfer functions can be extended into the Laplace domain with s [where $s = (-\xi + i)\omega$, ξ is the damping ratio of the motion] in (5) substituted for $i\omega$. The inverse Laplace transform yields the aerodynamic impulse function

$$I_{L_{seh}}(t) = A_1 \delta(t) + A_2 \frac{b}{U} \dot{\delta}(t) + A_3 \frac{b^2}{U^2} \ddot{\delta}(t)$$

$$+ \sum_{l=1}^{m} \int_{-\infty}^{t} A_{l+3} \exp \left(-\frac{d_l U}{b} (t - \tau) \dot{\delta}(\tau) \right) d\tau \tag{6}$$

where $\delta(t)$ = Dirac delta function.

Thus, the self-excited lift induced by arbitrary vertical motion can be expressed as

$$L_{seh}(t) = \frac{1}{2} \rho U^2 \left(A_1 h(t) + A_2 \frac{b}{U} \dot{h}(t) + A_3 \frac{b^2}{U^2} \ddot{h}(t) + \sum_{l=1}^{m} \phi_l(t) \right) \tag{7}$$

where $\phi_l(t)$ ($l = 1$ to m) are new variables that are introduced to express the aerodynamic phase lag and satisfy the following equations:

$$\dot{\phi}_l(t) = -\frac{d_l U}{b} \phi_l(t) + A_{l+3} \dot{h}(t), \quad (l = 1 \text{ to } m) \tag{8}$$

Similar formulations for other self-excited force components can be given with analogous definitions and are omitted here for the sake of brevity.

The buffeting forces per unit span corresponding to arbitrary wind fluctuations are expressed in terms of convolution integrals involving the aerodynamic impulse functions and fluctuating wind velocities

$$L_b(t) = -\frac{1}{2} \rho U^2 \int_{-\infty}^{t} \left(I_{L_{bu}}(t - \tau) \frac{u(\tau)}{U} + I_{L_{bw}}(t - \tau) \frac{w(\tau)}{U} \right) d\tau \tag{9a}$$

$$D_b(t) = \frac{1}{2} \rho U^2 \int_{-\infty}^{t} \left(I_{D_{bu}}(t - \tau) \frac{u(\tau)}{U} + I_{D_{bw}}(t - \tau) \frac{w(\tau)}{U} \right) d\tau \tag{9b}$$

$$M_b(t) = \frac{1}{2} \rho U^2 \int_{-\infty}^{t} \left(I_{M_{bu}}(t - \tau) \frac{u(\tau)}{U} + I_{M_{bw}}(t - \tau) \frac{w(\tau)}{U} \right) d\tau \tag{9c}$$

where I indicates the aerodynamic impulse functions of buffeting forces; the subscript represents the corresponding com-

ponent; and u and w = longitudinal and vertical components of the fluctuating wind velocity, respectively.

The buffeting forces per unit span are commonly expressed as follows:

$$L_b(t) = -\frac{1}{2}\rho U^2(2b)\left(2C_L\chi_{L_{bu}}\frac{u(t)}{U} + (C_L' + C_D)\chi_{L_{bw}}\frac{w(t)}{U}\right) \quad (10a)$$

$$D_b(t) = \frac{1}{2}\rho U^2(2b)\left(2C_D\chi_{D_{bu}}\frac{u(t)}{U} + C_D'\chi_{D_{bw}}\frac{w(t)}{U}\right) \quad (10b)$$

$$M_b(t) = \frac{1}{2}\rho U^2(2b)^2\left(2C_M\chi_{M_{bu}}\frac{u(t)}{U} + C_M'\chi_{M_{bw}}\frac{w(t)}{U}\right) \quad (10c)$$

where C_L, C_D, and C_M = mean lift, drag, and moment coefficients, respectively; $C_L' = dC_L/d\alpha$, $C_D' = dC_D/d\alpha$ and $C_M' = dC_M/d\alpha$; and $\chi_{L_{bu}}$, $\chi_{L_{bw}}$, $\chi_{D_{bu}}$, $\chi_{D_{bw}}$, $\chi_{M_{bu}}$, and $\chi_{M_{bw}}$ = aerodynamic transfer functions between fluctuating wind velocities and buffeting forces. These are functions of frequency and are dependent on the deck configuration. The absolute magnitudes of these functions are also referred to as aerodynamic admittance functions.

Following the approach used for the self-excited forces, the frequency dependent buffeting forces can be included in a time domain analysis. The Fourier transform of aerodynamic impulse functions of buffeting forces can be related to the aerodynamic transfer functions as follows:

$$\bar{I}_{L_{bu}} = 4bC_L\chi_{L_{bu}}; \quad \bar{I}_{L_{bw}} = 2b(C_L' + C_D)\chi_{L_{bw}} \quad (11a,b)$$

$$\bar{I}_{D_{bu}} = 4bC_D\chi_{D_{bu}}; \quad \bar{I}_{D_{bw}} = 2bC_D'\chi_{D_{bw}} \quad (11c,d)$$

$$\bar{I}_{M_{bu}} = 8b^2C_M\chi_{M_{bu}}; \quad \bar{I}_{M_{bw}} = 4b^2C_M'\chi_{M_{bw}} \quad (11e,f)$$

Accordingly, these can be expressed in terms of rational functions. For example, for the term corresponding to the lift induced by the vertical wind fluctuation $\bar{L}_{bw}(t)$

$$\bar{I}_{L_{bw}}(i\omega) = A_{w,1} + \sum_{l=1}^{m_w}\frac{A_{w,l+1}i\omega}{i\omega + \frac{d_{w,l}U}{b}} \quad (12)$$

The buffeting lift induced by arbitrary vertical wind fluctuation can then be given as

$$L_{bw}(t) = -\frac{1}{2}\rho U^2\left((A_{w,1} + A_{w,l+1})\frac{w(t)}{U} - \sum_{l=1}^{m_w}\frac{d_{w,l}U}{b}\phi_{w,l}(t)\right) \quad (13)$$

$$\dot{\phi}_{w,l}(t) = -\frac{d_{w,l}U}{b}\phi_{w,l}(t) + A_{w,l+1}\frac{w(t)}{U}, \quad (l = 1 \text{ to } m_w) \quad (14)$$

where $A_{w,1}$, $A_{w,l+1}$, and $d_{w,l}$ ($l = 1$ to m_w) = frequency independent coefficients; and $\phi_{w,l}$ ($l = 1$ to m_w) = additional variables. Similar formulations for other buffeting force components are omitted here for the sake of brevity.

The lift component of the self-excited and buffeting forces acting on the entire beam element with length L can be expressed as

$$L_{se}^e(t) = \int_0^L L_{se}(t)\ dx; \quad L_b^e(t) = \int_0^L L_b(t)\ dx \quad (15a,b)$$

The associated drag and moment can be expressed accordingly.

Since at this time there is not enough data for quantifying the spanwise correlation of the self-excited forces, without loss of generality, these are assumed to be fully correlated for the present study, and only the spanwise correlation of the buffeting forces is included. It is assumed that the stochastic properties of the buffeting force components per unit span at different positions within the same element are identical to those defined at the center of the element and that the correlation

between the buffeting force components induced by the u- and w-components are negligible. Thus, the self-excited and buffeting forces over the entire element are given

$$L_{se}^e(t) = L_{se}^c(t)L \quad (16a)$$

$$L_b^e(t) = L\int_0^t (J_{L_{bu}}(t - \tau)L_{bu}^c(\tau) + J_{L_{bw}}(t - \tau)L_{bw}^c(\tau))\ d\tau \quad (16b)$$

where the superscript c indicates the center of the element; $J_{L_{bw}}(t)$ and $J_{L_{bw}}(t)$ = impulse functions whose Fourier transform counterparts $\bar{J}_{L_{bw}}(\omega)$ and $\bar{J}_{L_{bw}}(\omega)$ are referred to as the joint acceptance functions defined as

$$\bar{J}_{L_{bw}}^2 = \frac{1}{L^2}\int_0^L\int_0^L coh_{L_{bw}}(x_1, x_2; f)\ dx_1\ dx_2 \quad (17)$$

where

$$coh_{L_{bw}}(x_1, x_2; f) = S_{L_{bw}}(x_1, x_2; f)/S_{L_{bw}^c}(f) \quad (18)$$

indicates the spanwise coherence of the buffeting lift force component $L_{bw}(t)$; $S_{L_{bw}}(x_1, x_2; f)$ indicates the cross-spectra between $L_{bw}(t)$ at two different positions denoted by the coordinates x_1 and x_2 along the bridge axis; and $S_{L_{bw}^c}(f)$ indicates the autospectral density of $L_{bw}^c(t)$. Other terms have analogous definitions but are omitted here for the sake of brevity. Several wind tunnel tests and full-scale experiments have indicated that the buffeting forces have a higher spanwise correlation than the incident wind fluctuations [e.g., Larose and Mann (1998)]. The joint acceptance functions also need to be expressed in terms of rational functions as shown before for other cases.

The solution of the equations of motion was obtained by the Newmark beta step-by-step integration method. The computational procedure for the aerodynamic forces was as follows. First, the wind fluctuations at the center of each element were simulated. The aerodynamic forces acting on each element were then calculated using the preceding expressions. The total nodal force vectors $\mathbf{F}_{se}$ and $\mathbf{F}_b$ were assembled from the element forces. The dependence of the aerodynamic characterisics on the initial static rotation of the bridge section can be included in the analysis. Because the self-excited forces are dependent on the unknown motion [(7)], they should be calculated iteratively at each time step until the required convergence criterion is satisfied. Although iterations are required, the process converges rapidly. The influence of the structural nonlinearities can also be readily included in the analysis.

Analysis in Modal Coordinates

For linear structures, a mode generalized approach offers computational efficiency because the analysis can be carried in the selected modes. The equations of motion in the generalized coordinates $\mathbf{q}$ are

$$\mathbf{M}_0\ddot{\mathbf{q}} + \mathbf{C}_0\dot{\mathbf{q}} + \mathbf{K}_0\mathbf{q} = \mathbf{Q}_{se} + \mathbf{Q}_b \quad (19)$$

where $\mathbf{M}_0 = \mathbf{\Psi}^T\mathbf{M}\mathbf{\Psi}$, $\mathbf{C}_0 = \mathbf{\Psi}^T\mathbf{C}\mathbf{\Psi}$, and $\mathbf{K}_0 = \mathbf{\Psi}^T\mathbf{K}\mathbf{\Psi}$ = generalized mass, damping, and stiffness matrices, respectively; $\mathbf{Q}_{se} = \mathbf{\Psi}^T\mathbf{F}_{se}$ and $\mathbf{Q}_b = \mathbf{\Psi}^T\mathbf{F}_b$ = generalized self-excited and buffeting force vectors, respectively; and $\mathbf{\Psi}$ = mode shape matrix.

The preceding equation is convenient for the analysis when aerodynamic force nonlinearities are included. However, an iterative procedure is required for calculating the self-excited forces at each time step, even for linear self-excited forces. For the case of linear self-excited forces, this iterative calculation can be eliminated by moving the self-excited force terms in (19) on the left-hand side and expressing the generalized self-excited forces as

$$Q_{se} = \frac{1}{2} \rho U^2 \left(\mathbf{A}_s \mathbf{q} + \frac{b}{U} \mathbf{A}_d \dot{\mathbf{q}} \right) \qquad (20)$$

where $\mathbf{A}_s$ and $\mathbf{A}_d$ = frequency dependent matrices that are functions of flutter derivatives and mode shapes.

The generalized self-excited forces, such as in the preceding section, can be approximated as a rational function

$$\mathbf{A}_{sd}(s) = \mathbf{A}_s + \frac{sb}{U} \mathbf{A}_d = \mathbf{A}_1 + \mathbf{A}_2 \left(\frac{sb}{U} \right) + \mathbf{A}_3 \left(\frac{sb}{U} \right)^2 + \sum_{l=1}^{m} \frac{\mathbf{A}_{l+3}s}{s + \frac{d_l U}{b}} \qquad (21)$$

where matrices $\mathbf{A}_1$, $\mathbf{A}_2$, $\mathbf{A}_3$, $\mathbf{A}_{l+3}$, and d_l ($d_l \geq 0$; $l = 1$ to m) are frequency independent coefficients. The preceding rational function representation can be directly derived from those of the nodal self-excited forces. However, for bridges with different aerodynamic characteristics along their axes, this would lead to a large number of additional equations needed to express the aerodynamic states. Instead of using an element-by-element description of nodal forces in terms of rational functions, the rational function for the generalized self-excited forces can be determined by fitting the tabular data of the generalized forces at different reduced velocities.

By taking the Laplace transform of (19) and (20), substituting (21), and subsequently introducing additional variable vectors representing the unsteady aerodynamic states $\mathbf{q}_{sel}$ ($l = 1$ to m), the following is obtained:

$$s^2 \bar{\mathbf{M}} \mathbf{q}(s) = \{ -s\bar{\mathbf{C}} - \bar{\mathbf{K}} \} \mathbf{q}(s) + \frac{1}{2} \rho U^2 \sum_{l=1}^{m} \mathbf{q}_{sel}(s) + \mathbf{Q}_b(s) \qquad (22)$$

$$\mathbf{q}_{sel}(s) = \frac{\mathbf{A}_{l+3}s}{s + \frac{U}{b} d_l} \mathbf{q}(s), \quad (l = 1 \text{ to } m) \qquad (23a,b)$$

where $\bar{\mathbf{M}} = \mathbf{M}_0 - (1/2)\rho b^2 \mathbf{A}_3$, $\bar{\mathbf{C}} = \mathbf{C}_0 - (1/2)\rho U b \mathbf{A}_2$, and $\bar{\mathbf{K}} = \mathbf{K}_0 - (1/2)\rho U^2 \mathbf{A}_1$.

The following set of state-space equations that describe the system dynamics can be obtained by taking the inverse Laplace transform

$$\dot{\mathbf{Y}} = \mathbf{A}\mathbf{Y} + \mathbf{B}\mathbf{Q}_b \qquad (24)$$

where

$$\mathbf{Y} = \begin{Bmatrix} \mathbf{q} \\ \dot{\mathbf{q}} \\ \mathbf{q}_{sel} \\ \vdots \\ \mathbf{q}_{sem} \end{Bmatrix} \qquad (25a)$$

$$\mathbf{A} = \begin{bmatrix} \mathbf{0} & \mathbf{I} & \mathbf{0} & \cdots & \mathbf{0} \\ -\bar{\mathbf{M}}^{-1}\bar{\mathbf{K}} & -\bar{\mathbf{M}}^{-1}\bar{\mathbf{C}} & \frac{1}{2}\rho U^2 \bar{\mathbf{M}}^{-1} & \cdots & \frac{1}{2}\rho U^2 \bar{\mathbf{M}}^{-1} \\ \mathbf{0} & \mathbf{A}_4 & -\frac{U}{b}d_1\mathbf{I} & \cdots & \mathbf{0} \\ \vdots & \vdots & \vdots & & \vdots \\ \mathbf{0} & \mathbf{A}_{3+m} & \mathbf{0} & \cdots & -\frac{U}{b}d_m\mathbf{I} \end{bmatrix} \qquad (25b)$$

$$\mathbf{B} = \begin{bmatrix} \mathbf{0} \\ \bar{\mathbf{M}}^{-1} \\ \mathbf{0} \\ \vdots \\ \mathbf{0} \end{bmatrix} \qquad (25c)$$

Both the buffeting response and flutter instability can be analyzed in the time domain using the preceding frequency independent state-space equation in a numerical integration scheme. In the present study, a fourth-order Runge-Kutta scheme is utilized. The flutter analysis can be conducted by neglecting the buffeting force components to get the information on frequencies, damping ratios, and mode shapes from the free vibration response. Because the unsteady self-excited forces are implicitly included in the coefficient matrix, the iterative calculation for the self-excited forces at each time step is unnecessary. In addition, the flutter analysis can also be performed by the complex eigenvalue analysis (Chen et al. 2000).

SIMULATION OF CORRELATED WIND VELOCITY TIME HISTORIES

The multidimensional multivariate wind velocity time histories with prescribed spectral characteristics along the bridge axis were generated using an autoregressive scheme (Li and Kareem 1990)

$$\begin{Bmatrix} \mathbf{u}(t) \\ \mathbf{w}(t) \end{Bmatrix} = \sum_{k=1}^{m} \mathbf{C}(k) \begin{Bmatrix} \mathbf{u}(t - k\Delta t) \\ \mathbf{w}(t - k\Delta t) \end{Bmatrix} + \mathbf{N}(t) \qquad (26)$$

where $\mathbf{u}(t)$ and $\mathbf{w}(t)$ = longitudinal and vertical wind fluctuation vectors, respectively; $\mathbf{C}$ = coefficient matrix; $\mathbf{N}(t)$ = white noise process vector; Δt = time interval; and m = filter order.

The power spectral density components of the $\mathbf{u}$ and $\mathbf{w}$ vectors used herein are given by the von Kármán spectra (Chen et al. 2000). The coherence functions between the u- and w-components were neglected, and those between different u-components or w-components are given by

$$coh_r(x_i, x_j; f) = \exp \left(-\frac{\lambda_r |x_i - x_j|}{2\pi L_r^x} 0.747 \sqrt{1 + 70.78 \left(\frac{fL_r^x}{U} \right)^2} \right) \qquad (27)$$

where r represents u and w; L_r^x = integral scales of wind fluctuations in the crosswind direction; λ_r = decay factor; and x_i and x_j = coordinates along the bridge axis.

RATIONAL FUNCTION APPROXIMATION

This section details the rational function representation of the aerodynamic characteristics (i.e., the flutter derivatives, admittance function, and spanwise coherence). For an airfoil, the rational function representation of the Theodorsen function/Wagner function and Sears function/Küssner function are widely utilized. To validate the accuracy of the rational function representation in expressing the frequency dependent characteristics of unsteady aerodynamic forces on bluff bridge
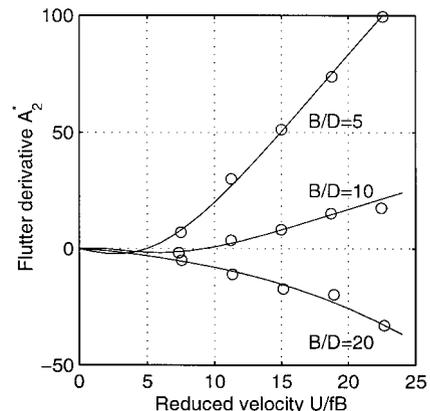

FIG. 2. Rational Function Approximation of A_2^* for Rectangular Sections: ———, Fitting; ○, Experimental Data

sections, rectangular cross sections with aspect ratios of B/D = 5, 10, and 20 (B = body width; D = body depth) are employed for which experimental data are available (Matsumoto et al. 1995). Fig. 2 shows the measured flutter derivative A_2^* along with those derived from rational function representation with two lag terms [(5)]. The results exhibited a good match, which suggests that the self-excited forces on bluff body sections can be expressed by the rational function with good accuracy.

The aerodynamic transfer function between the wind fluctuations and buffeting forces are generally complex functions of the reduced frequency. Because there are not enough experimental data available for identifying the phase shift between the wind fluctuations and the buffeting forces, real functions were assumed, without loss of generality, for the rational function approximation. Nonetheless, the phase shift information can be readily incorporated when the experimental data become available. Fig. 3 shows the results of the rational function representation for the admittance function given by the following expression (Davenport 1962):

$$\chi^2 = \frac{2}{c^2}\,(c - 1 + e^{-c}) \tag{28}$$

where $c = \lambda\,fD/U$; D = section depth; λ = decay factor that is assumed to be 8. The results suggested a good fit to the target values.

Fig. 4 shows the result of the rational function approximation for the joint acceptance function. The coherence of the buffeting forces was assumed to be the same as those for the wind fluctuations [(27)]. Accordingly, the joint acceptance functions for an element of length L are given by
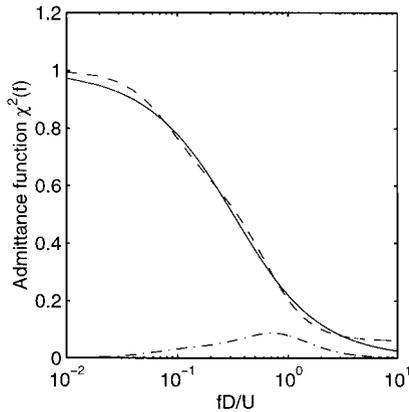
FIG. 3. Rational Function Approximation of Admittance Function: ——, Target; – – –, Fitting (Real Part); –·–, Fitting (Imaginary Part)
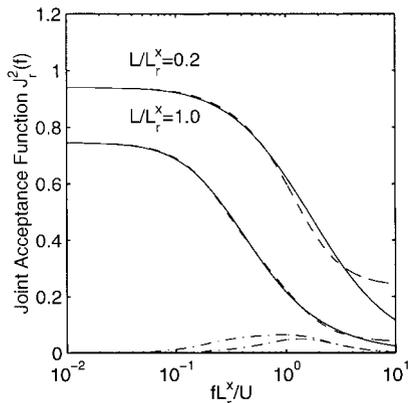

FIG. 4. Rational Function Approximation of Joint Acceptance Function: ——, Target; – – –, Fitting (Real Part); –·–, Fitting (Imaginary Part)

$$J_r^2 = \frac{2}{s_r^2}\,(s_r - 1 + e^{-s_r}) \tag{29a}$$

$$s_r = \frac{\lambda_r L}{2\pi L_r^x}\,0.747\,\sqrt{1 + 70.78\left(\frac{fL_r^x}{U}\right)^2} \tag{29b}$$

where λ_r = decay factor and is assumed to be 8; and r indicates the symbols u and w. Based on the results presented here, it was concluded that the frequency dependent unsteady aerodynamic characteristics of bluff bridge sections can be described accurately in terms of rational functions.

EXAMPLE

An example long span suspension bridge with a main span of approximately 2,000 m was used to predict the flutter and buffeting response. The logarithmic damping ratio for each mode was assumed to be 0.02. Only the aerodynamic forces acting on the bridge deck were considered, and the variation of the aerodynamic characteristics with the static rotation were ignored here for simplicity and without loss of generality. The aerodynamic parameters are $C_D = 0.3230$, $C_D' = 0$, $C_L = 0.0942$, $C_L' = 1.905$, and $C_M = 0.0104$, $C_M' = 0.2717$; H_1^* to H_4^* and A_1^* to A_4^* are evaluated using the Theodorsen function; P_1^* to P_6^*, A_5^*, A_6^*, H_5^*, H_6^* are based on the quasi-steady theory: $P_1^* = -2C_D/k$, $P_2^* = (C_L - C_D')/(2k)$, $P_3^* = C_D'/k^2$, $P_5^* = (C_D' - C_L)/k$, $H_5^* = 2C_L/k$, $A_5^* = -4C_M/k$, and $P_4^* = P_6^* = H_6^* = A_6^* = 0$; $\chi_{D_{bu}}$ and $\chi_{D_{bw}}$ were based on (28); $\chi_{L_{bu}}$, $\chi_{L_{bw}}$, $\chi_{M_{bu}}$, and $\chi_{M_{bw}}$ were given by the Sears function; the spanwise correlation of buffeting forces was assumed to be the same as the corresponding wind fluctuations (i.e., $coh_{L_{bu}} = coh_{D_{bu}} = coh_{M_{bu}} = coh_u$, $coh_{L_{bw}} = coh_{D_{bw}} = coh_{M_{bw}} = coh_w$); $\sigma_u/U = 10\%$; $\sigma_w/U = 5\%$; $L_u^x = L_u^y = 80$ m; $L_w^x = L_w^y = 40$ m; and $\lambda_u = \lambda_w = 8$.

Flutter Analysis

Flutter analysis was conducted in the time domain by calculating the free vibration response using (24) (i.e., time domain scheme a) and (19) (i.e., time domain scheme b). With scheme a, the generalized self-excited forces were calculated based on the rational function representation. In this scheme, the iterative calculation for self-excited forces is unnecessary. With scheme b, the generalized self-excited forces were calculated through the nodal forces that were calculated based on the rational function presentation with iterative calculations at each time step. For linear cases, both schemes provide the same results, with scheme a being more efficient. The first 15 modes were included in the analysis. To calculate the free vibration response dominated by a certain mode, only the appropriate modal coordinate was given a small initial velocity or displacement, and all other initial displacements and velocities were set equal to zero. Examples of the torsional displacement at the center of the main span at wind velocities of 40 and 70 m/s with an initial velocity imparted to mode 10 are shown in Fig. 5. For comparison, the coupled multimode flutter analysis was also conducted by the solution of the com-
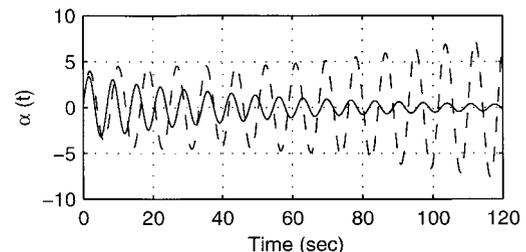

FIG. 5. Examples of Free Vibration of Torsional Displacement at Center of Main Span: ——, $U = 40$ m/s; – – –, $U = 70$ m/s

plex eigenvalues of the system described by (24). Two cases were considered. First, only the symmetric first, second, and third vertical modes and symmetric first torsional mode (i.e., modes 2, 8, 10, and 11) were included. The second case included the first 15 lower natural modes. The variation of frequencies and damping ratios obtained by the time domain and frequency domain approaches are shown in Figs. 6 and 7, respectively. The comparison of the flutter condition is given in Table 1. It is noted that the time domain approaches predict the flutter conditions in good agreement with those from the frequency domain approach. In this example, the damping of the mode with the coupled vertical and torsional motions turns to negative beyond the mean wind velocity of about 69 m/s. In other words, the coupled flutter occurs and the structure becomes unstable. For the linear case, the flutter analysis in the frequency domain is very computationally efficient when compared with the time domain approaches. However, the

time domain approach permits incorporation of nonlinear aerodynamic forces or structural nonlinearities.

Buffeting Response

A number of samples of simulated wind fluctuations at the center of each element along the bridge axis at each wind velocity were simulated. The corresponding buffeting responses were calculated and compared with those from the frequency domain approach, including the aerodynamic coupling (Chen et al. 2000).

For the sake of brevity, only the results corresponding to the center of the main span are shown here. An example realization of the longitudinal and vertical wind fluctuations acting on the center of the main span at a wind velocity of 60 m/s is shown in Fig. 8. The autoregressive model coefficients were determined to generate 120 s of time histories at increments of 0.1 s. For brevity, comparison of simulated and target spectral characteristics was not included here. These results were in excellent agreement.

Figs. 9 and 10 show the corresponding unsteady self-excited and buffeting forces acting on the element at the center of the main span, respectively. Comparisons of their spectra calculated from the simulated time histories and based on the frequency domain formulations are shown in Figs. 11 and 12. The spectral descriptions of the self-excited and buffeting forces in the frequency domain approach are given as

$$S_{M_{se}^e} = \left(\frac{1}{2}\rho U^2 L\right)^2 (|\bar{I}_{M_{seh}}|^2 S_{hh} + \bar{I}_{M_{seh}}\bar{I}_{M_{sep}}^* S_{hp} + \bar{I}_{M_{seh}}^* \bar{I}_{M_{sep}} S_{hp}^*$$

$$+ \bar{I}_{M_{seh}}\bar{I}_{M_{se\alpha}}^* S_{h\alpha} + \bar{I}_{M_{seh}}^* \bar{I}_{M_{se\alpha}} S_{h\alpha}^* + |\bar{I}_{M_{sep}}|^2 S_{pp} + \bar{I}_{M_{sep}}\bar{I}_{M_{se\alpha}}^* S_{p\alpha}$$

$$+ \bar{I}_{M_{sep}}^* \bar{I}_{M_{se\alpha}} S_{p\alpha}^* + |\bar{I}_{M_{se\alpha}}|^2 S_{\alpha\alpha}) \qquad (30)$$

$$S_{M_b^e} = \left(\frac{1}{2}\rho U^2 L\right)^2 (2b)^4 [4C_M^2|\chi_{Mu}|^2|\bar{J}_u|^2 S_{uu}/U^2$$

$$+ C_M'^2|\chi_{Mw}|^2|\bar{J}_w|^2 S_{ww}/U^2] \qquad (31)$$

where S_{rs} $(r, s = h, p, \alpha)$ = power spectral components of the response; S_{uu} and S_{ww} = power spectra of the u- and w-components; and asterisk ($*$) denote the complex conjugate operator. Good agreement was noted, which further validates the technique that simulates the arbitrary aerodynamic forces using a rational function approximation.

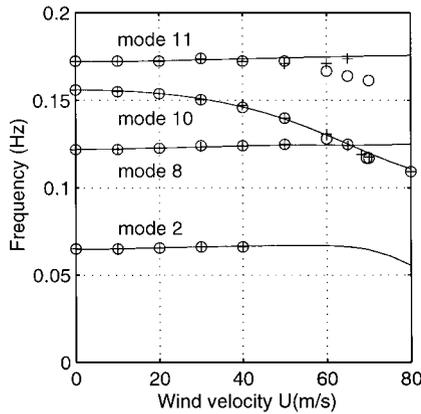Fig. 13 shows the vertical, lateral, and torsional responses

FIG. 6. Frequency versus Wind Velocity: ——, Frequency Domain; +, Time Domain Scheme a; ○, Time Domain Scheme b
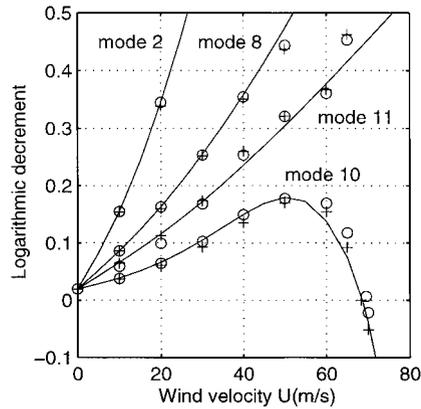

FIG. 7. Damping Ratio versus Wind Velocity: ——, Frequency Domain; +, Time Domain Scheme a; ○, Time Domain Scheme b

TABLE 1. Comparison of Flutter Conditions

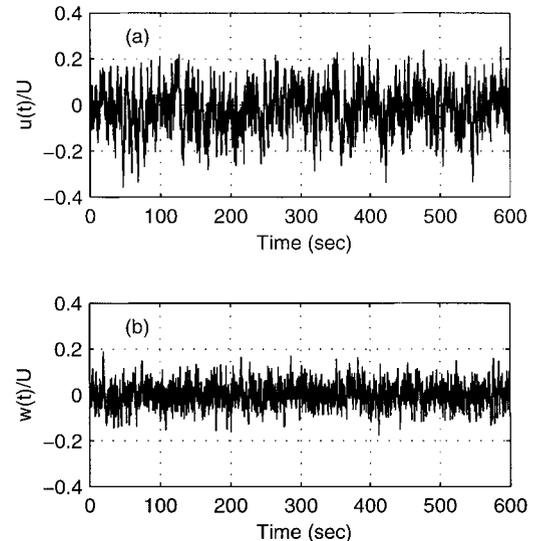| Mode number (1)	Onset velocity (m/s) (2)	Frequency (Hz) (3)
(a) Frequency domain		
Modes 2, 8, 10, and 11	68.6	0.1214
Modes 1–15	69.3	0.1188
(b) Time domain scheme a		
Modes 1–15	68.3	0.1190
(c) Time domain scheme b		
Modes 1–15	69.5	0.1170

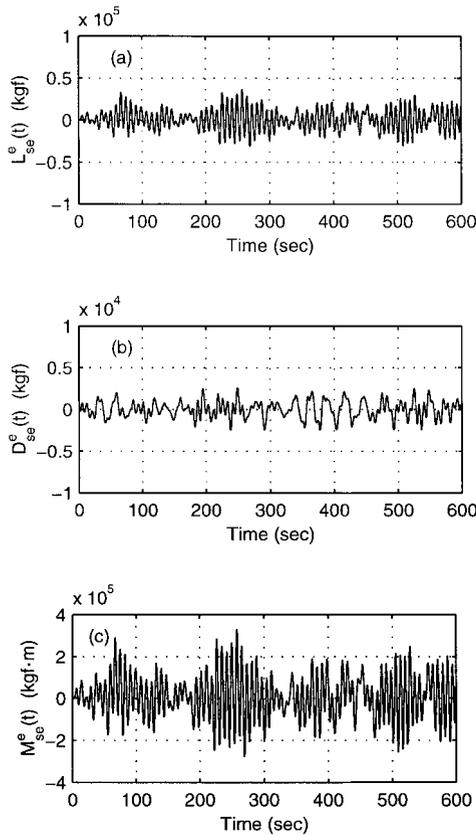**FIG. 8. Example of Simulated Wind Fluctuations ($U = 60$ m/s): (a) Longitudinal Component; (b) Vertical Component**

FIG. 9. Self-Excited Forces on Element at Center of Main Span (U = 60 m/s): (a) Lift; (b) Drag; (c) Moment

FIG. 10. Buffeting Forces on Element at Center of Main Span (U = 60 m/s): (a) Lift; (b) Drag; (c) Moment

evaluated in the time domain at a wind velocity of 60 m/s using schemes a and b. Both results are nearly coincident so that the distinction cannot be made from these figures. In the following discussion, unless specifically noted, scheme a is used for buffeting response analysis. In Fig. 14, the response at 70 m/s is presented and clearly demonstrates the occurrence of coupled flutter.

Fig. 15 shows a comparison of the RMS vertical, lateral, and torsional displacement at the center of the main span. The results from frequency domain analysis are indicated by the solid lines, and the time domain results are indicated by the mean values and the 99% confidence intervals [$\mu - 2.58\sigma$ $\mu + 2.58\sigma$] (μ and σ are the mean value and standard deviation, respectively). The time domain results show very good agreement with those from the frequency domain approach in the vertical and torsional directions, although the lateral responses are slightly smaller than those from the frequency domain approach. This validates the proposed time domain approach using frequency dependent aerodynamic parameters. This approach can be extended to include nonlinearities of both aerodynamic and structural origins, which are intractable in the conventional frequency domain approaches.

The effects of the aerodynamic coupling on the buffeting response are further investigated by neglecting the aerodynamic coupling, that is, dropping the off-diagonal components of the aerodynamic self-excited force matrices $\mathbf{A}_s$ and $\mathbf{A}_d$ [(20)]. Fig. 16 shows the torsional displacement at wind velocities of 60 and 70 m/s without aerodynamic coupling excited by the same wind fluctuations (Fig. 8). The RMS of torsional displacement at different wind velocities is shown in Fig. 17, compared with the results from frequency domain analysis with aerodynamic coupling indicated by the solid line. Significant underestimation in the higher wind velocities is noted by comparing the results shown in Figs. 13–15 in which
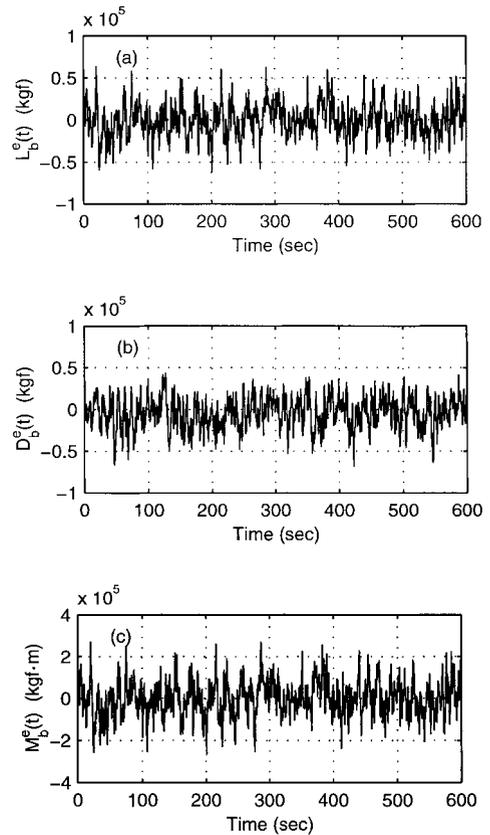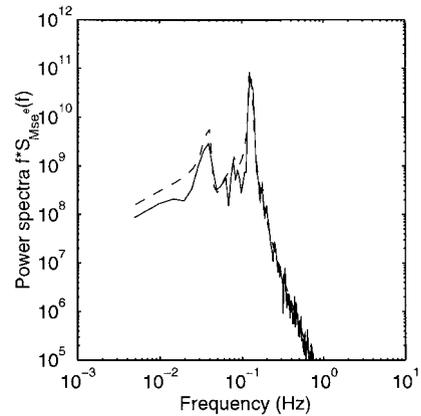

FIG. 11. Comparison of Power Spectra of Self-Excited Moment (U = 60 m/s): ———, Time Domain; ———, Frequency Domain
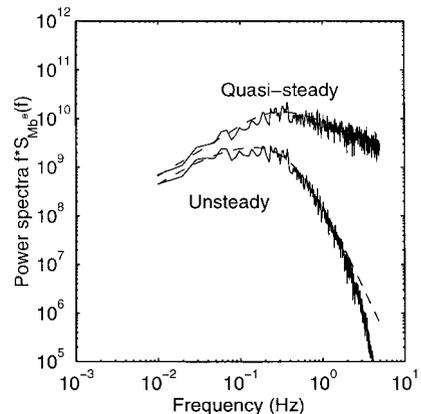

FIG. 12. Comparison of Power Spectra of Buffeting Moment (U = 60 m/s): ———, Time Domain; ———, Frequency Domain
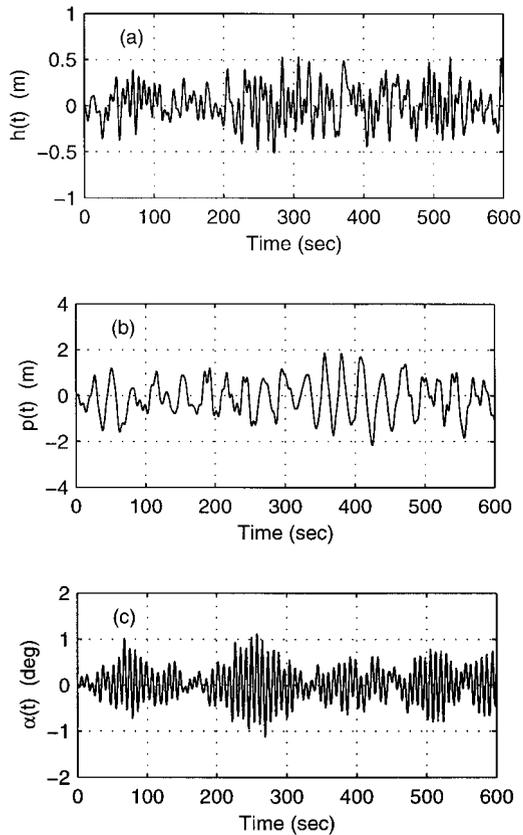
FIG. 13. Buffeting Response at Center of Main Span (U = 60 m/s): (a) Vertical; (b) Lateral; (c) Torsional Displacements (——, Time Domain Scheme a; ———, Time Domain Scheme b)
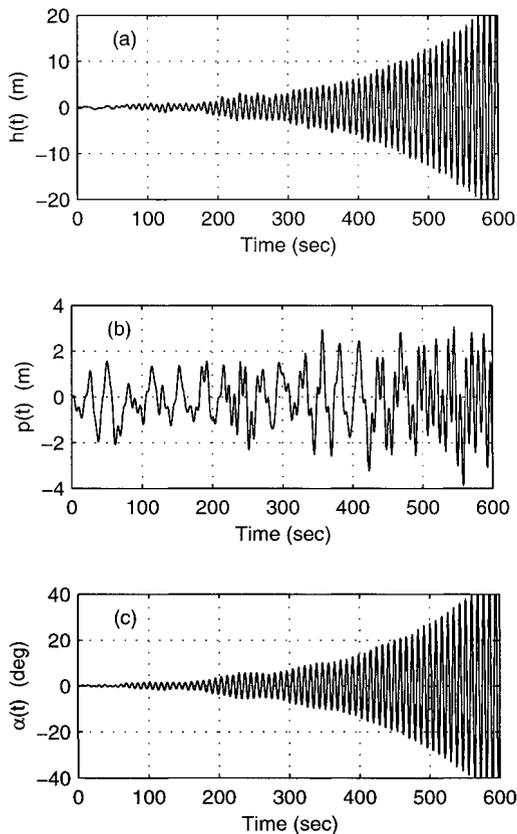

FIG. 14. Buffeting Response at Center of Main Span (U = 70 m/s): (a) Vertical; (b) Lateral; (c) Torsional Displacements
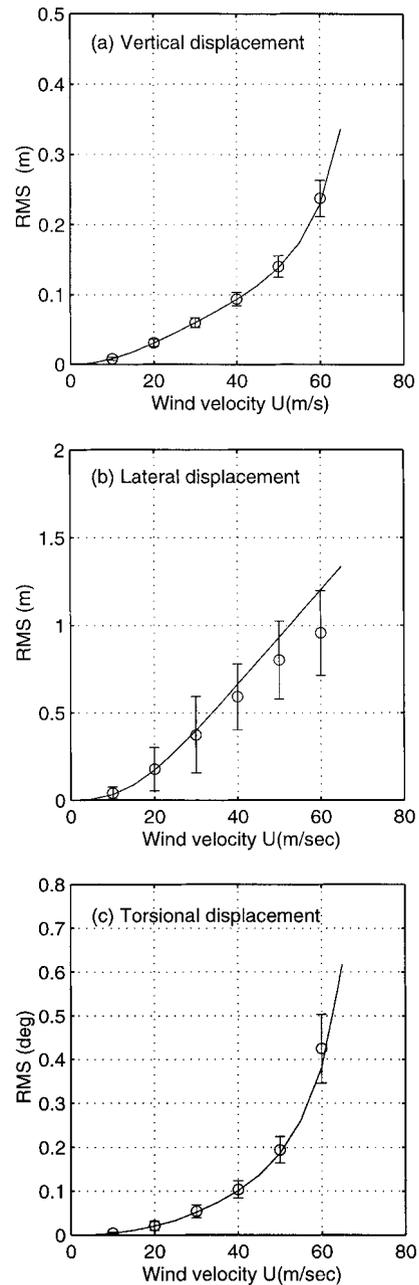

FIG. 15. RMS of Displacements at Center of Main Span: (a) Vertical; (b) Lateral; (c) Torsional Displacements

the aerodynamic coupling effects are included. Coupled flutter cannot be observed without aerodynamic coupling effects.

To investigate the effects of the unsteady characteristics of buffeting forces on the buffeting response, the analysis using the quasi-steady buffeting forces is also conducted by setting the admittance function and joint acceptance function equal to unity. Figs. 18 and 19 show, respectively, the quasi-steady buffeting moment and the torsional displacement at the center of the main span at a wind velocity of 60 m/s, which are clearly higher in the quasi-steady approach. Fig. 20 shows the RMS of torsional displacement at different wind velocities using the quasi-steady buffeting forces, compared with the results from the frequency domain analysis using unsteady forces. It should be noted that because the buffeting forces are overestimated by the quasi-steady theory, conservative results are observed. However, when the self-excited forces are also modeled by the quasi-steady theory as most of the time domain studies entail, the aerodynamic damping will be overestimated, which leads to an underestimation of the response. Nonetheless, it is clear
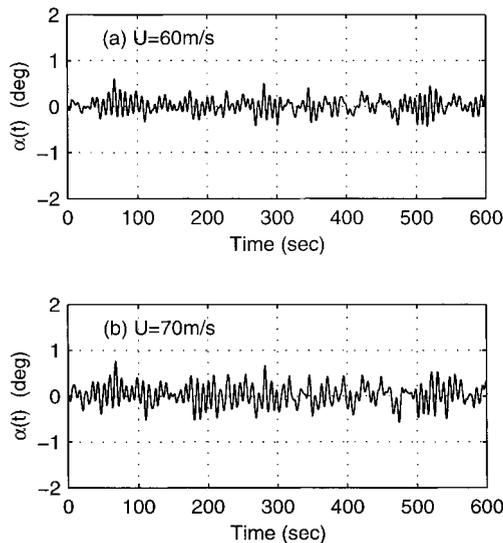
FIG. 16. Buffeting Torsional Displacement without Aerodynamic Coupling: (a) *U* = 60 m/s; (b) *U* = 70 m/s
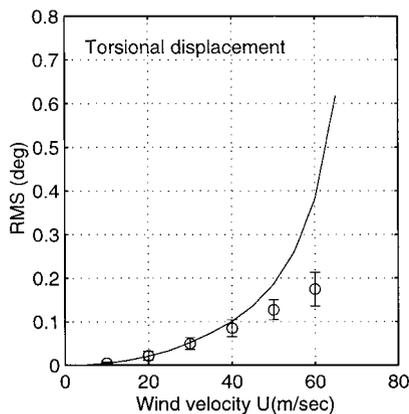

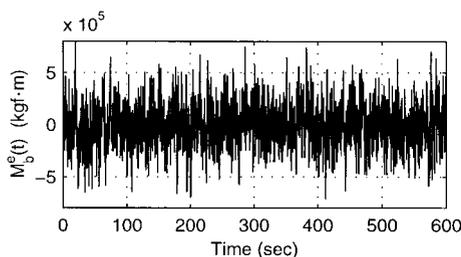FIG. 17. RMS of Torsional Displacement without Aerodynamic Coupling

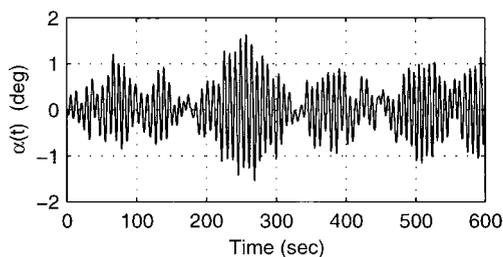FIG. 18. Quasi-Steady Buffeting Moment at Element of Center of Main Span (*U* = 60 m/s)

FIG. 19. Buffeting Torsional Displacement Using Quasi-Steady Buffeting Forces (*U* = 60 m/s)
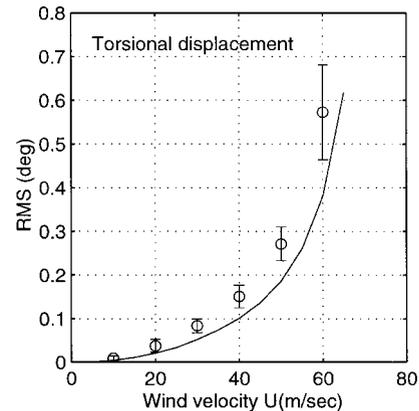

FIG. 20. RMS of Torsional Displacement Using Quasi-Steady Buffeting Forces

that using quasi-steady aerodynamic forces, the buffeting response at higher wind velocity and the flutter instability cannot be evaluated accurately.

CONCLUSIONS

A time domain approach to calculate the flutter and buffeting response of long span bridges is presented. The unsteady aerodynamic self-excited forces and buffeting forces are used instead of the quasi-steady force formulation customarily used in the conventional time domain approaches. Unsteady wind forces are expressed in terms of the convolution integrals involving the aerodynamic impulse functions and the structural motions or wind fluctuations. The aerodynamic impulse functions and the associated aerodynamic transfer functions are approximated in terms of rational functions. These functions can be determined from experimentally derived flutter derivatives, admittance functions, and the spanwise coherence of aerodynamic forces. Utilizing an example bridge, the flutter and buffeting response based on the time domain approach is compared with a frequency domain analysis that includes the contribution of coupled aerodynamic self-excited forces. The response shows very good comparison. The aerodynamic coupling and the unsteady characteristics of the buffeting forces influence the buffeting response significantly. The time domain approach offers the benefit of capturing the effects of nonlinearities of both structural and aerodynamic origins and also the influence of nonstationary features in the approaching wind in the analysis.

ACKNOWLEDGMENTS

APPENDIX. REFERENCES

Agar, T. T. A. (1988). "The analysis of aerodynamic flutter of suspension bridges." *Comp. and Struct.*, 30, 593–600.

Chen, X., Matsumoto, M., and Kareem, A. (2000). "Aerodynamic coupling effects on the flutter and buffeting of bridges." *J. Engrg. Mech.*, ASCE, 126(1), 17–26.

Davenport, A. G. (1962). "Buffeting of a suspension bridge by stormy winds." *J. Struct. Div.*, ASCE, 88(3), 233–268.

Diana, G., Bruni, S., Collina, A., and Zasso, A. (1998). "Aerodynamic challenges in super long span bridges design." *Bridge aerodynamics*, Larsen and Esdahl, eds., 131–144.

Jain, A., Jones, N. P., and Scanlan, R. H. (1996). "Coupled flutter and buffeting analysis of long-span bridges." *J. Struct. Engrg.*, ASCE, 122(7), 716–725.

Katsuchi, H., Jones, N. P., and Scanlan, R. H. (1999). "Multimode coupled flutter and buffeting analysis of the Akashi-Kaikyo Bridge." *J. Struct. Engrg.*, ASCE, 125(1), 60–70.

Kovacs, I., Svensson, H. S., and Jordet, E. (1992). "Analytical aerodynamic investigation of cable-stayed Helgeland Bridge." *J. Struct. Engrg.*, ASCE, 118(1), 147–168.

Larose, G. L., and Mann, J. (1998). "Gust loading on streamlined bridge decks." *J. Fluids and Struct.*, 12, 511–536.

Li, Y., and Kareem, A. (1990). "ARMA system in wind engineering." *Probabilistic Engrg. Mech.*, 5(2), 50–59.

Li, Y., and Kareem, A. (1993). "Simulation of multivariate random processes: Hybrid DFT and digital filtering approach." *J. Engrg. Mech.*, ASCE, 119(5), 1078–1098.

Lin, Y. K., and Yang, J. N. (1983). "Multimode bridge response to wind excitations." *J. Engrg. Mech.*, ASCE, 109(2), 586–603.

Matsumoto, M., Chen, X., and Shiraishi, N. (1994). "Buffeting analysis of long span bridge with aerodynamic coupling." *Proc., 13th Nat. Symp. on Wind Engrg.*, Japan Association for Wind Engineering, 227–232 (in Japanese).

Matsumoto, M., Niihara, Y., Kobayashi, Y., Shirato, H., and Hamasaki, H. (1995). "Flutter mechanism and its stabilization of bluff bodies." *Proc., 9th ICWE*, 827–838.

Roger, K. L. (1977). "Airplane math modeling methods for active control design." AGARD-CP-228.

Santos, J. C., Miyata, T., and Yamada, H. (1993). "Gust response of a long span bridge by the time domain approach." *Proc., APSOWE 3*, 137–142.

Scanlan, R. H. (1978). "The action of flexible bridges under wind. 2: Buffeting theory." *J. Sound and Vibration*, 60(2), 201–211.

Scanlan, R. H. (1984). "Role of indicial functions in buffeting analysis of bridges." *J. Struct. Engrg.*, ASCE, 110(7), 1433–1446.

Scanlan, R. H., Béliveau, J.-G., and Budlong, K. S. (1974). "Indicial aerodynamic functions for bridge decks." *J. Engrg. Mech.*, ASCE, 100(4), 657–672.

Shinozuka, M., and Jan, C. M. (1972). "Digital simulation of random processes and its applications." *J. Sound and Vibration*, 25(1), 111–128.

Xiang, H. F., Liu, C. H., and Gu, M. (1995). "Time domain analysis for coupled buffeting response of long span bridges." *Proc., 9th ICWE*, 881–892.